Received: 7 June 2022 | Revised: 7 September 2022 | Accepted: 12 September 2022

DOI: 10.1049/rpg2.12598

IET Renewable Power Generation

The Institution of Engineering and Technology WILEY

ORIGINAL RESEARCH

The performance analysis of the low-speed direct-drive generators for harvesting current energy

Po-Yu Chen[1] | **Kung-Yen Lee**[1,2] | **Po-Chun Huang**[1] | **Jia-Han Li**[1] | **Forng-Chen Chiu**[1] | **Jing-Fa Tsai**[1] | **Shu-Ting Hsu**[1]

[1]Department of Engineering Science and Ocean Engineering, National Taiwan University, Taipei, Taiwan

[2]Advanced Research Center for Green Materials Science and Technology, National Taiwan University, Taipei, Taiwan

Correspondence
Kung-Yen Lee, Department of Engineering Science and Ocean Engineering, National Taiwan University, Taipei 10617, Taiwan.
Email: kylee@ntu.edu.tw

Abstract

The simulations and experiments for two 400 W low-speed direct-drive permanent magnet synchronous generators (PMSGs) installed in a Floating Kuroshio Turbine (FKT) were implemented. The towing tank experiments were carried out at National Taiwan University. A generator can start to harvest current energy at the rotation speed of 30 rpm (corresponding to the current flow rate of 0.36 m/s), and produce the rated power of 400 W at 150 rpm. The speed is very low compared with the published reports. The energy conversion efficiency of the FKT is up to 0.85. The results show that the generated direct current (DC) power is more than 800 W at a flow rate of 1.5 m/s. The power coefficient for the FKT is about 0.4. The energy loss at each stage and the power difference between the testing platform and the towing tank experiment were also analyzed. Moreover, the shape of the FKT is a new design. Compared with other structures, the proposed FKT can easily follow the direction of the ocean current and the depth of the FKT can be adjustable; when it doesn't operate, it will float on the surface so that it is easy for maintenance.

1 | INTRODUCTION

As global warming becomes worse, the emission of CO_2 must be significantly reduced. Consequently, the development of renewable energy is urgently needed. One of the methods to produce energy is to utilize the ocean current. The advantages of current power plants are clean, sustainable, carbon-free, and pollution-free. In addition, marine energy is autonomous and independent of supplies from overseas, thereby ensuring energy security.

When generating marine energy, the current flow rate is one of the key parameters related to the kinetic energy of the current. Furthermore, the density of seawater (1030 kg/m^3) is about 858 times higher than the density of air (1.20 kg/m^3). Therefore, the energy density of the kinetic energy generated by the ocean current can reach the same level as a wind turbine at a much lower flow rate.

Because the ocean has an enormous potential for generating energy [1], numerous research teams have made various developmental background analyses and assessments into ocean current power generation [2–4].

Currently, the development of a proper environment that extracts marine energy from the current has been investigated in areas such as Taiwan [5], Japan [6, 7], Florida (USA) [8–10], and Ireland [11]. The tidal current turbine, SeaGen in Ireland, has two generators with gearboxes [11]. The SeaGen U with three 1 MW turbines is developed for water depth exceeding 35 m. The support structure is fixed on the bottom of the ocean. In addition, the SeaGen F is developed with two 1 MW turbines for the floating deployment application. Therefore, the depth of SeaGen U and F cannot be adjusted, compared with the proposed structure.

Japanese research teams have made studies into harvesting energy from the Kuroshio current. For example, K. Shirasawa from Okinawa proposed a new ocean-current turbine that has an unconventional shape to operate a turbine in the middle layer of a marine current [12]. As it is necessary to cancel the resulting rotor torque, the turbine is therefore designed with a

float at the top and a counterweight at the bottom. The turbine maintains a stable position thanks to buoyancy and gravity. The system only has one 1 kW generator which is not a direct drive and the rated rotation speed is 458 revolutions per minute (rpm). The float on the top and the counterweight on the bottom of the turbine is to balance the rotation caused by the torque when the turbine operates. There is only one generator and a counterweight on the bottom in the system, compared with the proposed structure. In addition, the New Energy and Industrial Technology Development Organization (NEDO) in Japan was also dedicated to developing Kuroshio turbines. They have completed a 100 kW floating type of ocean current power generation system, "Kairyu", which was tested in the actual Kuroshio current off the coast of Kuchinoshima, Toshima, in the Kagoshima Prefecture [13–15]. Kairyu has two generators (100 kW) and three nacelles. The middle nacelle has the capability of diving depth adjustment and power transform. The other nacelles have two generators installed. There is not a lateral foil float, compared with the proposed structure. Ueno reported the development construction and demonstration of the floating type ocean current turbine system. It achieved the installation procedure feasibility, submergence height, attitude stability and power output of 70–90 kW at a flow rate of 1.5 m/s due to the flow fluctuation turbulence velocities etc. [15]. The research team from the University of Tokyo also investigated the background of the turbulence around Kuchinoshima [16]. Some companies in Japan have developed a twin-turbine floating-type system that has a weathervane function, where the depth is controlled by adjusting the buoyancy and the blade pitch [17, 18]. They have conducted research into the device stability and the cable stress of the ocean current turbine system [19]. Moreover, the motion of the twin-turbine system concerning the starting conditions was analyzed [20]. The adjustment of the blade pitch angles in different conditions in the real ocean was also simulated [21]. The research team at Wanchi Steel Corporation in Taiwan successfully generated an average power of 26.31 kW with a flow rate of 1.27 m/s from the Kuroshio current [22].

For a regular generator, a gearbox connected blades and a generator is used to increase the rotation speed and then drive the generator to produce power. However, the gearbox will cause power loss and damage during the conversion. For a direct-drive low-speed generator, the generator can be directly driven by the blade at relatively low speed. Wei reported that the low-speed generator has an efficiency of 85.5% at 200 rpm which is higher than the proposed rotation speed of 150 rpm [23]. S. Tanigaki reported a water bearing, drive train and prototype testing of the ocean current turbine in Kuroshio current. The rated power output is 20 kW at a flow rate of 1.5 m/s [24]. The rated rotation speed is 47.7 rpm. It also has two generators and a buoyancy body [24] which is also different from the proposed FKT in this article. Wei reported that two 1 kW direct-drive low-speed and high-efficiency PM generators using silicon steel and Common Cold Steel Plate (SPCC) were simulated, fabricated and compared [23]. The generator can generate about 959 W at 200 rpm and the efficiency is about 86.4% at 200 rpm. The load is 160 Ω and the voltage is about 343 V at 200 rpm [23]. Han reported that a 5 kW distributed ocean current energy hydrostatic transmission (HST) power generation with a dual-pump confluence design, can efficiently generate power in a low flow rate and deep environment. The working pressure of the HST is reduced to avoid overflow and the dispersed micro-energy in the deep sea can be aggregated together to active power [25]. Jiang reported a hybrid ocean wave-current energy converter (HWCEC) which can harvest energy from waves and current simultaneously with a single power take-off. The current energy is extracted by using a current turbine. Experimental results validate the dynamic modelling and show the HWCEC can increase the output power between 24% and 89% over either the current turbine or wave energy converter [26]. Weiss proposed a methodological approach to identify potential zones for wind and wave energy exploitation, using long-term data series with fine spatial and temporal resolution. For wave energy, Brazil and New Zealand present good opportunities for the development of wave energy, with an estimated extractable power of 372 TWh/month and 286 TWh/month, respectively [27].

However, many studies into the Kuroshio current are only in the research stage, so few data describe the actual power generation efficiency corresponding to the flow rate of Kuroshio. This paper is focused not only on simulations, but also on the actual generation of power from towing tank experiments. The proposed current turbine is designed to harvest Kuroshio current energy because the Kuroshio current is about 30 km away from the eastern coast of Taiwan, and the flow rate of the current is up to 1.5 m/s, which is very suitable for developing a Kuroshio current power plant. Consequently, we propose a floating Kuroshio turbine (FKT) system that considers the low-speed direct-drive generator concept. The innovations of the proposed system are: (1) The FKT system will be attached to the middle layer of the ocean using a single mooring line, and its buoyancy and gravity will be adjusted to control the working depth corresponding to the Kuroshio flow rate. This novel design allows the FKT system to float to the surface of the ocean for maintenance when the turbines do not operate, or automatically dive to a deeper layer when the turbine operates. This is because the force caused by the rotation of the blade overcomes the buoyancy. Therefore, the FKT system can prevent damage during serious weather conditions, including the effect of waves on the efficiency. (2) Another innovation is that the generator is the low-speed direct-drive type so that it can produce power at a relatively low speed (~30 rpm, corresponding to the current flow rate of 0.36 m/s) and the rated power of 400 W at 150 rpm. (3) In addition, the shape of the Floating Kuroshio Turbine with a foil float is a new design, which makes the FKT maintain a stable position under the sea, compared with the Kuroshio turbine, Kairyu. (4) The concept of a low-speed direct-drive generator will reduce the requirement and cost of maintenance because the FKT system doesn't contain a gearbox.

The proposed 800 W FKT is composed of two 400 W permanent magnet synchronous generators (PMSGs). The 400 W

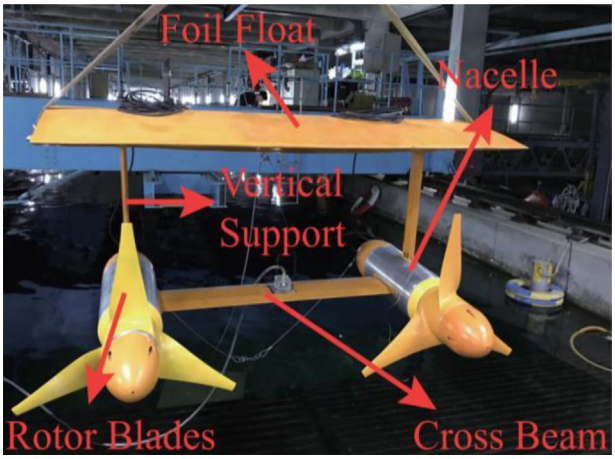

FIGURE 1 An 800 W floating kuroshio turbine

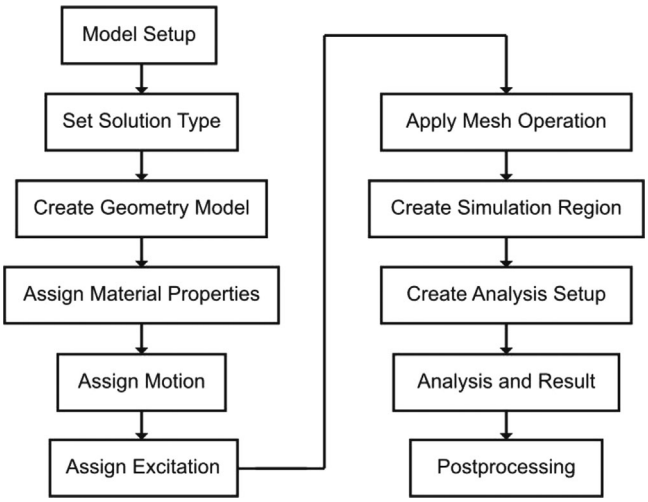

FIGURE 2 Simulation procedure

low-speed direct-drive PMSG was designed using finite element analysis software. The components parameters, such as materials, winding types, the dimensions of the stator and rotor, the mesh density, etc. were designed and simulated [28, 29]. After fabrication, the 400 W low-speed direct-drive PMSGs were tested using a testing platform. Finally, we also conducted an underwater towing tank experiment of the FKT at the Department of Engineering Science and Ocean Engineering, National Taiwan University. The performance of the FKT system was measured and analyzed at various flow rates. The picture of the proposed FKT is shown in Figure 1, which is described in Section 4.

2 | FINITE ELEMENT SIMULATION

2.1 | Design and simulation of the PMSG

Figure 2 shows the design procedure for the simulation presented in this paper. The PMSG structure was designed in SolidWorks and imported into the ANSYS Maxwell software. The model for the 400 W AC inner rotor PMSG was divided into six parts including the core, the outer covering, the rotor, the stator, the winding coil, and the permanent magnet, as shown listed in Table 1. The inner diameter of the rotor is 25 mm; the outer diameter is 114.5 mm; the inner diameter of the stator is 116 mm; and the air gap is 1.5 mm. In addition, the PMSG has 20 poles at 25 Hz and 24 slots, and is a concentrated winding type. The type of steel is 50CS400 grade with a N45H type magnet. A Y-connection external circuit was used in the Maxwell Circuit Editor. The generator is rated at 150 rpm and can output a rated power of 400 W. In this simulation, at least 500 steps within 1 s were used to ensure the simulation quality and accuracy.

TABLE 1 Parameters of a PMSG

Item	Values
Machine	PMSG
Rotor position	Inner rotor
Reference speed (rpm)	150
Rated Power (W)	400
Rated Phase Voltage (V)	128.45
Rated Phase Current (A)	1.01
Torque Constant (Nm/A)	27.93
Flux linkage λ_m (Wb)	1.2
Control type	AC
Frequency (Hz)	25
Number of poles	20
Number of slots	24
Steel Type	50CS400
Magnet Type	N45H
Rotor outer diameter (mm)	114.5
Stator inner diameter (mm)	116
Winding type	Concentrated
Connecting type	Y connecting

2.2 | Simulation results

The simulation results for the 400 W low-speed direct-drive PMSG show that the alternative current (AC) power output was then rectified by the full wave bridge rectifier circuit which is composed of 6 diodes, 3 parallel capacitors and an 182 Ohms resistor, as shown in Figure 3. According to the simulation results, DC output voltage and current were 270 V and 1.48 A, respectively. The simulated power output is the product of the DC voltage and the DC current. The power output curve is shown in Figure 4, which is about 398 W with a load of 182 Ohms at 150 rpm, close to the target of 400 W. The average torque is 27.66 N m at steady state, as shown in Figure 5. From the relationship of torque, speed and power, the power output at 150 rpm is 434 W, also close to the target.

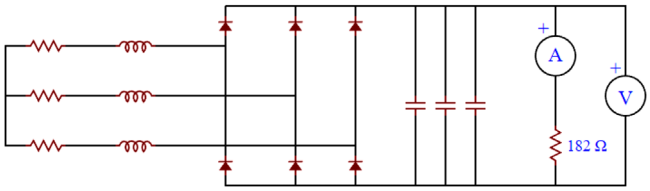

FIGURE 3 The simulated external circuit of DC power

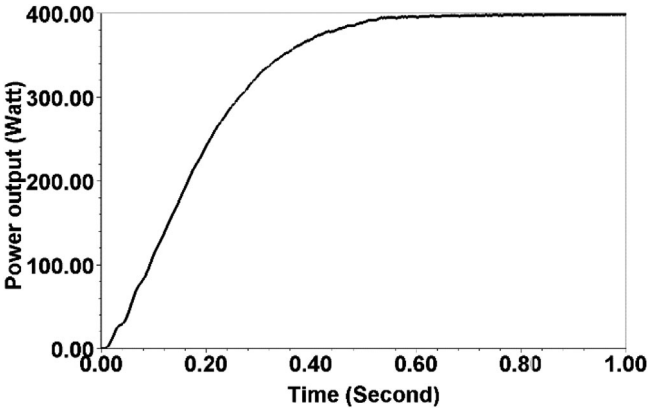

FIGURE 4 Simulated DC power

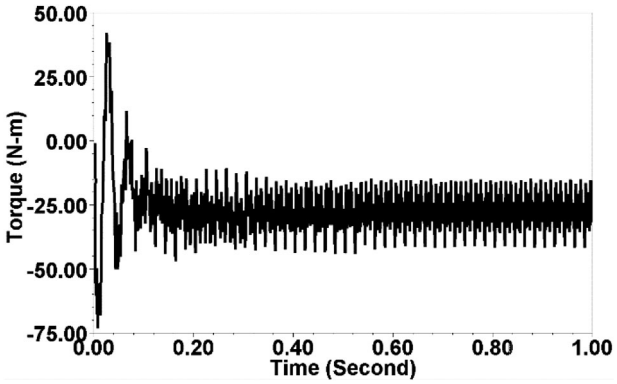

FIGURE 5 Simulated PMSG torque

In addition, the magnetic field intensity and the magnetic flux density was also investigated since the proper magnetic field intensity can prevent magnetic saturation and increase PMSG efficiency at different rotation speeds. After simulation, the change in magnetic flux density and magnetic field intensity were quite linear as the rotation speed increased. The maximum flux density was about 1.8 Tesla at 100 rpm and 2.1 Tesla at 150 rpm. From the *B–H* curve, the PMSG has the proper magnetic flux density without inducing magnetic saturation, as shown in Figure 6.

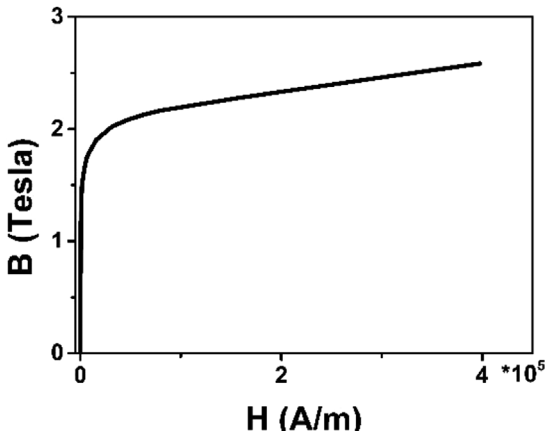

FIGURE 6 Simulated *B–H* curve for the PMSG

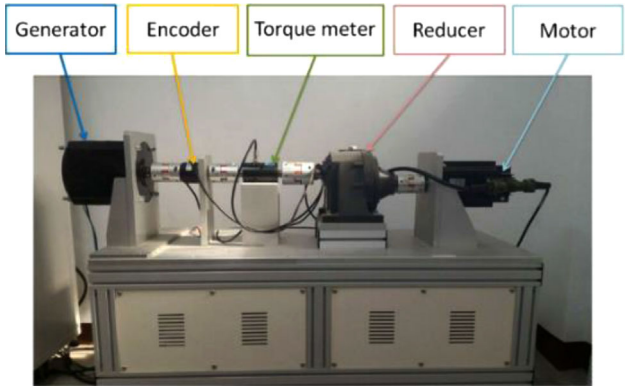

FIGURE 7 Illustration of the testing platform [30]

3 | TESTING OF TWO PMSGS

3.1 | Testing platform

The two PMSGs, denoted as PMSG-1 and PMSG-2, were tested on a testing platform that was composed of a motor, a reducer, a torque meter, and an encoder, as shown in Figure 7 [30]. The motor was controlled by the computer in order to ensure that it rotates at the required speed. The reducer then reduces the rotation speed and increases the torque, which can ensure that the PMSGs are rotated and then produce AC power output. The AC power output is transferred to a DC power output using a full bridge rectifier circuit. The values of the torque and the rotation speed of the PMSGs are measured using a torque metre and an encoder. The power between the AC–DC transformation increases from 0 to 25 W as the rotation speed increases from 30 to 150 rpm. The generated power follows two equations below:

$$P = I^2\mathrm{R} = \mathrm{IV} \tag{1}$$

$$P = \frac{T \cdot n}{9549} \tag{2}$$

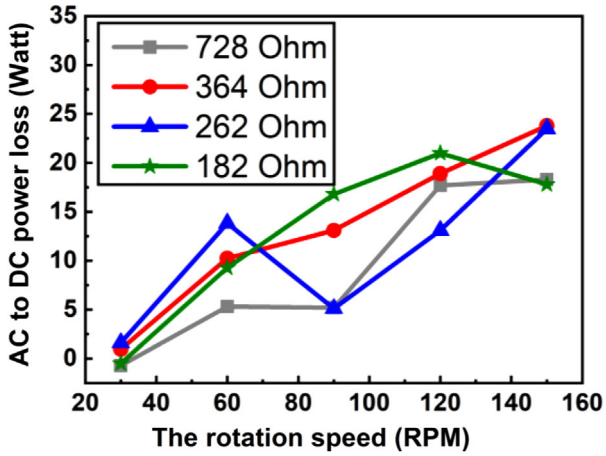

FIGURE 8 Power loss for PMSG-1 in AC–DC transformation

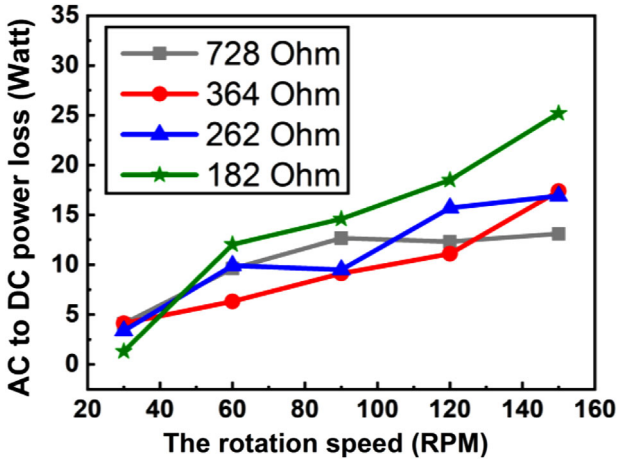

FIGURE 9 Power loss for PMSG-2 in AC–DC transformation

where P is power; I is current; R is resistance; V is voltage; T is torque and n is rotation speed.

3.2 | Testing results

Figures 8 and 9 show the power loss for PMSG-1 and PMSG-2 in the AC–DC transformation at rotation speeds between 30 and 150 rpm with the loads of 728, 364, 262, and 182 Ohms. The calculated internal resistance is about 15 Ohms at around 150 rpm. Both PMSG-1 and PMSG-2 are able to generate power more than 400 W. In addition, it can be seen from Figure 9 that PMSG-2 is more stable. The power loss at a load of 182 Ohms and a higher speed is higher than that at a load of 728 Ohms and a lower speed, as shown in Figures 8 and 9. This is because current increases with increasing speed and lower resistance so that the power loss on the internal resistance increases.

Figures 10 and 11 show the DC power output as a function of the rotation speed. The experiments were started at a speed of 30 rpm, which was then increased by 10 rpm for each step.

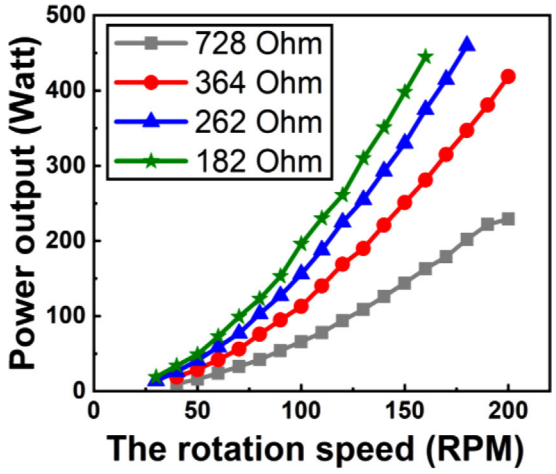

FIGURE 10 DC Power output for PMSG-1 tested by using the testing platform

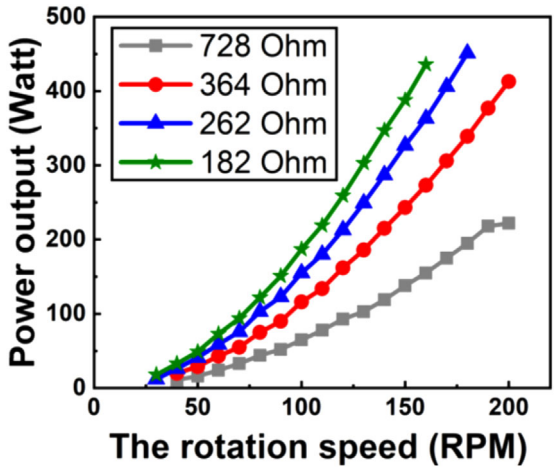

FIGURE 11 DC Power output for PMSG-2 tested by using the testing platform

The experiments were stopped once the power output reached 450 W in order to avoid overheating and damage. The power output for both PMSG is about 400 W with a load of 182 Ohms at 150 rpm. Both PMSGs can even reach about 450 W with a load of 182 Ohms at 160 rpm. In addition, both PMSGs can also generate over 400 W at about 170 rpm with a load of 262 Ohms. It can be seen that the power output for both PMSGs is similar.

Figures 12 and 13 show the torque of the PMSG as a function of the rotation speed tested by using the testing platform. Comparing Figures 10 and 11 with Figures 12 and 13, the rated power, 400 W, can be generated at different speeds, torques and loads. In general, the power and torque increase as the rotation speed increases and the resistance reduces. For example, the rated power can be generated by PMSG-2 at 150 rpm using 182 Ohms and a torque of 30 N m, or at 170 rpm using 262 Ohms and 28 N m. In order to obtain as much Kuroshio current energy as possible, particularly when the flow rate is between 1.0 and 1.5 m/s, not only do we need to generate 400 W at

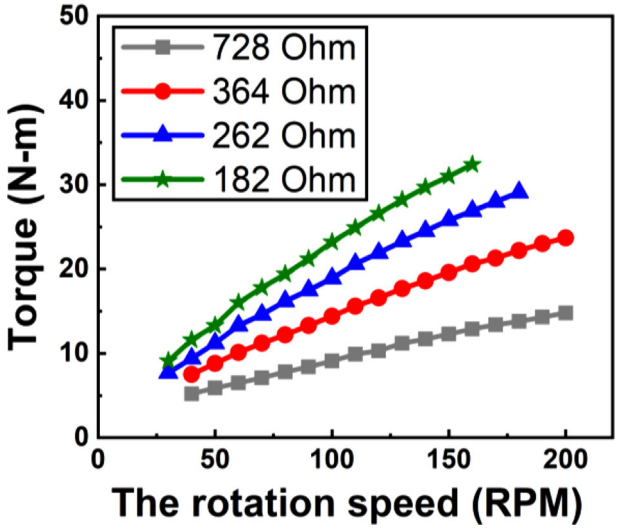

FIGURE 12 Torque for PMSG-1 measured by using the testing platform

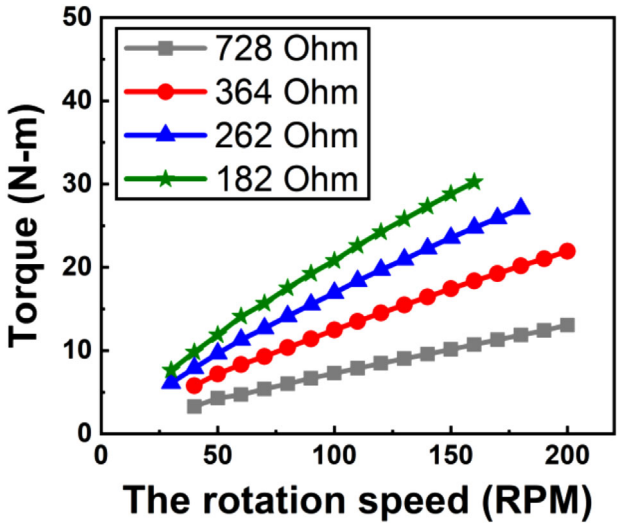

FIGURE 13 Torque for PMSG-2 measured by using the testing platform

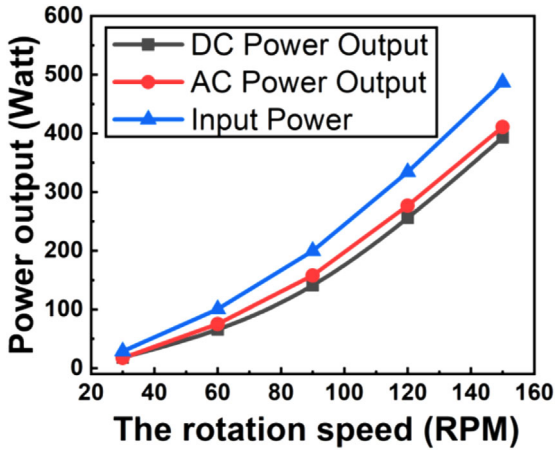

FIGURE 14 Comparison of the PMSG-1 input, the AC power and the DC power output at a load of 182 Ohms

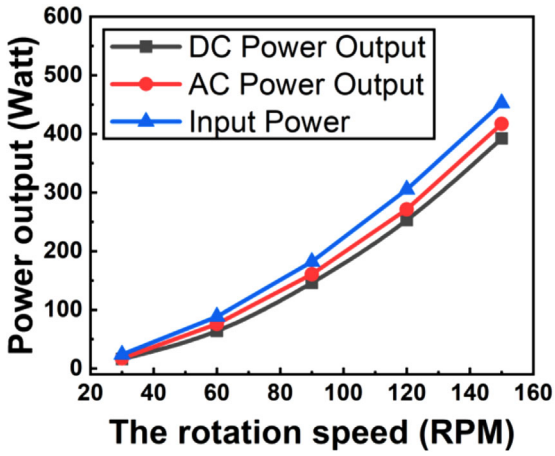

FIGURE 15 Comparison of the PMSG-2 input, the AC power and the DC power output at a load of 182 Ohms

150 rpm, but the torque also needs to be above 25 N m at 150 rpm. This is because the energy that can be captured from the Kuroshio current is strongly dependent on the length of the blades, which is relative to the torque. If the torques of both the PMSG and the blades don't match, the PMSGs may not work well and the efficiency may be very low. The relationship is shown in Equation (2).

Figures 14 and 15 show the comparison of the input, the AC power output and the DC power output of PMSG-1 and PMSG-2 with a load of 182 Ohms only. The input power was calculated by multiplying the PMSG torque and the rotation speed, shown as the line with a solid blue triangle. The AC power output was directly measured from the AC 3-phase outlet on the PMSG, shown as the line with a solid red circle. The third curve is the DC power output measured from the full bridge rectifier circuits, shown as the line with a solid green square. From these figures, we can easily observe the loss at each stage. The loss between the input and AC power output originates from the mechanical energy being converted to electrical energy. The energy conversion loss to the PMSG-1 is greater than that of the PMSG-2 because the higher PMSG-1 torque requires a greater input power. Furthermore, the energy loss between the AC output and the DC output is derived from the internal resistance of the rectifier circuits.

Figures 16 and 17 show the percentage of power loss from AC to DC, the mechanical input to the AC output, and the total power loss as a function of the rotation speed measured by using the testing platform at a load of 182 Ohms. In general, the percentage of power loss decreases as the rotation speed is increased, and the best performance occurs at the rated rotation speed. In addition, the difference between the input and the AC output for the PMSG-1 at a load of 728 Ohms at 150 rpm is 26.3%, which then decreases to 15.6% when the load decreases to 182 Ohms. The difference for PMSG-2 at a load of 728 Ohms at 150 rpm is 8.5%, which then decreases to 7.8% when the load decreases to 182 Ohms. Furthermore, the biggest difference between the AC output and the DC output for PMSG-2

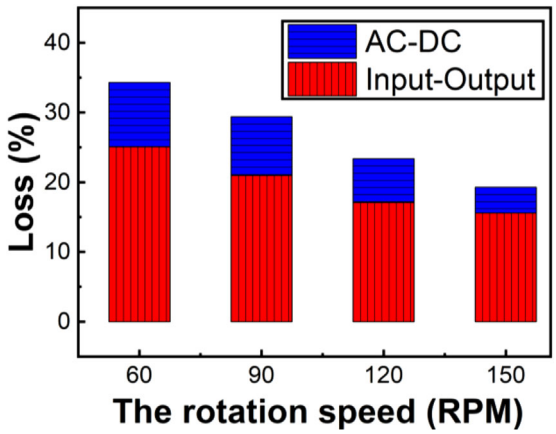

FIGURE 16 The percentage of power loss for PMSG-1 at a load of 182 Ohms

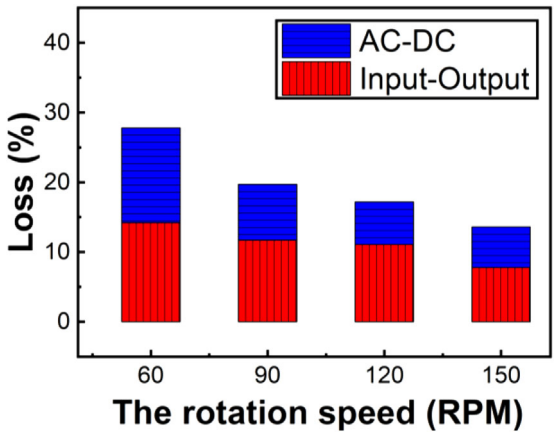

FIGURE 17 The percentage of power loss for PMSG-2 at a load of 182 Ohms

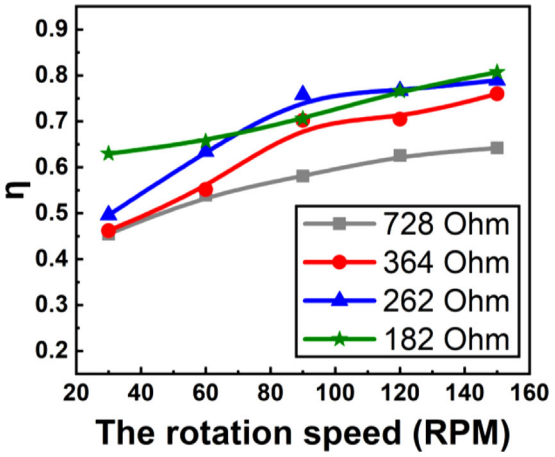

FIGURE 18 Efficiency of PMSG-1 by using the testing platform

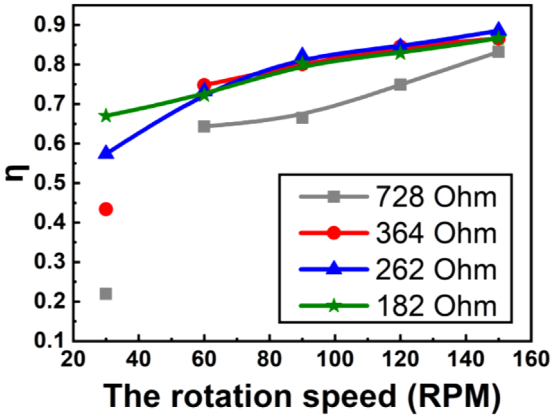

FIGURE 19 Efficiency of PMSG-2 by using the testing platform

is 15.8% at 60 rpm, which then decreases to 9% at 90 rpm, 6.8% at 120 rpm, and 6% at 150 rpm at a load of 182 Ohms. The biggest difference for PMSG-1 is 12.3% at 60 rpm, which decreases to 10.6% at 90 rpm, 7.6% at 120 rpm, and 4.3% at 150 rpm at a load of 182 Ohms. The total difference between the input power and the DC output power amounts to 19.3% for PMSG-1 and 13.3% for PMSG-2 at a load of 182 Ohms at 150 rpm.

Figures 18 and 19 show the energy conversion efficiency of the PMSGs, calculated by using the ratio of the mechanical energy of the motor to the output of the PMSG. The difference between both PMSGs at a low rotation speed is relatively larger. This situation is improved when each PMSG is operated at a higher rotation speed, especially around the rated rotation speed of 150 rpm. The efficiency of PMSG-1 increases with the increasing rotation speed. The highest energy conversion efficiency of 0.8 is obtained at a load of 182 Ohms at 150 rpm. However, the highest energy conversion efficiency achieved by PMSG-2 was about 0.85 at a rated rotation speed of 150 rpm at a load of 182 Ohms. As mentioned in the Introduction, there are only few research reports focused on a similar system under the different situations. The published report has an efficiency of 85.5% at 200 rpm with a load of 160 Ohms [30]. The difference in efficiency between these two PMSGs may derive from the different PMSG torque levels because a higher PMSG torque requires a higher mechanical input energy at the same rotation speed. Therefore, PMSG-2 has a higher power output than PMSG-1 at the same rotation speed, as shown in Figures 14 and 15, which means that PMSG-2 has better energy conversion efficiency.

$$Error\ (\%) = \frac{P_{simulaition} - P_{testing}}{P_{testing}} \tag{3}$$

Figures 20 and 21 show the simulated and measured DC power output for the PMSGs from 30 to 150 rpm. Also, the loads for the full wave bridge rectifier circuit connected to the AC power output for both simulation and the testing platform are 182, 262, 364, and 728 Ohms, respectively. It is obvious that the simulation results are very close to the measured results at different rotation speeds, particularly at the rated rotation speed of 150 rpm. The biggest error between the simulated power output and the measured power output calculated using

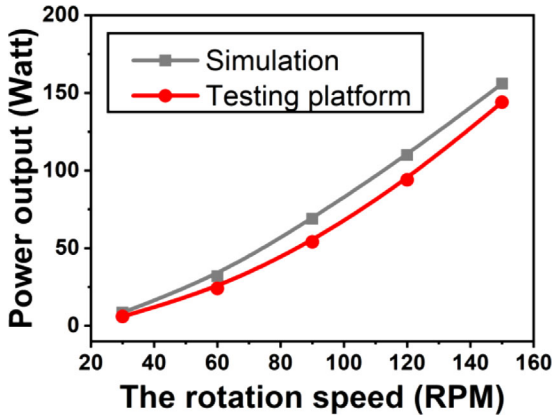

FIGURE 20 Simulated and tested DC power output for PMSG-1 at a load of 728 Ohms

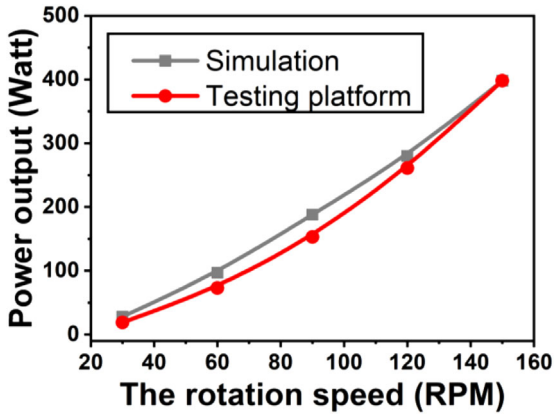

FIGURE 21 Simulated and tested DC power output for PMSG-1 at a load of 182 Ohms

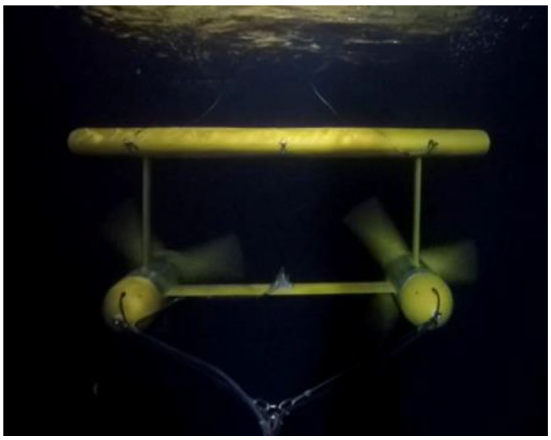

FIGURE 22 The floating turbine dives into the water when the generator operates

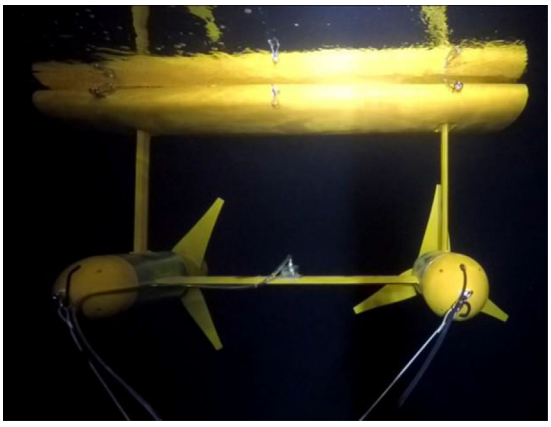

FIGURE 23 The floating turbine floats on the surface when the generator does not operate

Equation (3) appears at 728 Ohms and becomes smaller when the load reduces to 182 Ohms because the PMSG is designed to operate at a speed of 150 rpm. The errors at 728 Ohms range from 41.7% to 8.3%, as shown in Figure 20. The biggest error is 41.7% at 30 rpm, which decreases to 33% at 60 rpm, 27.8% at 90 rpm, 17% at 120 rpm, and 8.3% at 150 rpm. The errors at 182 Ohms range from 47.4% to 0.3%, as shown in Figure 21. The biggest error is 47.4% at 30 rpm, which decreases to 32.3% at 60 rpm, 22.9% at 90 rpm, 7.3% at 120 rpm, and 0.3% at 150 rpm.

4 | FLOATING KUROSHIO TURBINE

4.1 | Introduction to the floating Kuroshio turbine

Because the proposed FKT is moored by a single line, so that it can easily follow the direction of the Kuroshio current. In addition, the two turbines are the downwind type so that the FKT can easily adjust any current direction. Furthermore, the rotation directions of the blades of the two generators are counter-rotating and the FKT has the foil float on the top so that the design can make the FKT maintain a stable position under the sea. In this work, the relationship between the rotation speeds of the generators and power output is analyzed so that the influence of turbulence, wave, wake and current direction on the power output and efficiency are significantly alleviated.

In general, the flow rate of Kuroshio current is between 1.0 and 1.5 m/s, and the average flow rate is about 1.2 m/s. For safety and efficiency reasons, the rated speed has to be set at the upper limit. Otherwise, when the real Kuroshio flow rate is more than the rated speed, the turbine will be damaged and the generated power will be relatively lower. According to Figures 22–25, power output at different flow rates, with different loads, and at the average flow rate of 1.2 m/s was measured. Two generators can produce power output of 800 W, achieving the desired power output of this work.

Figure 1 in Introduction shows the 800 W FKT which includes a foil float, vertical supports, a cross beam, rotor blades, and a nacelle. The foil float is a wing-shaped design that creates lift when the current flows through the FKT. The vertical supports are used to connect the foil float and the nacelle. The

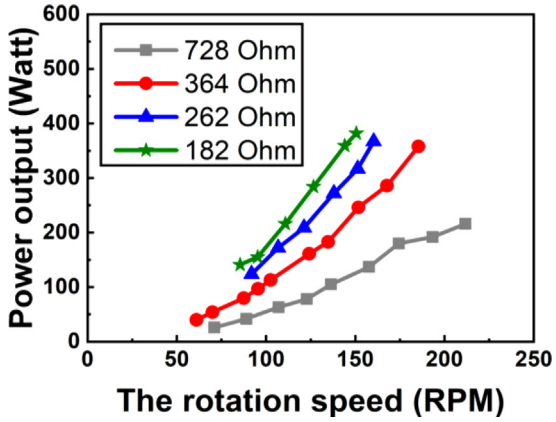

FIGURE 24 Power generation achieved by PMSG-1 during the towing experiments

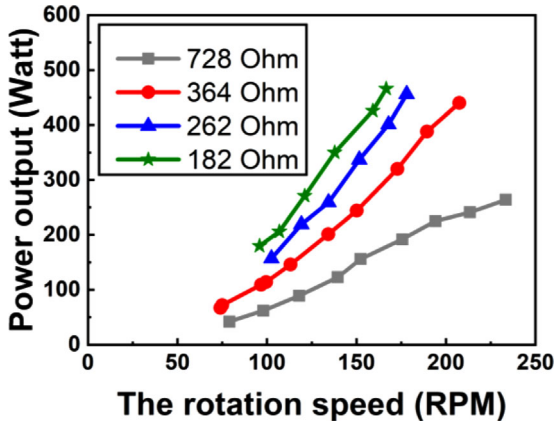

FIGURE 25 Power generation achieved by PMSG-2 during the towing experiments

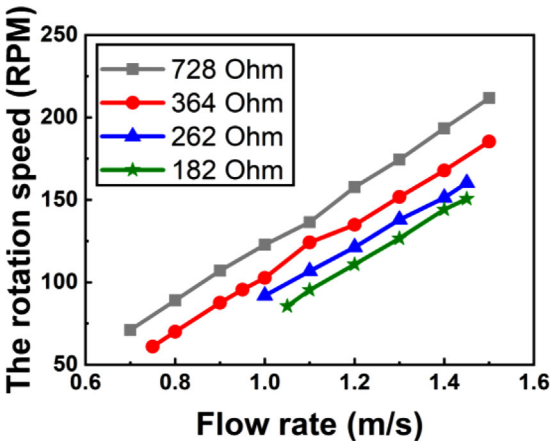

FIGURE 26 The rotation speed achieved by PMSG-1 versus the flow rate during the towing experiments

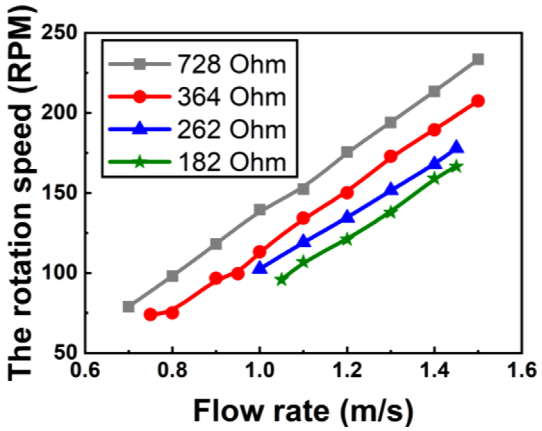

FIGURE 27 The rotation speed achieved by PMSG-2 versus the flow rate during the towing experiments

rotor blades are rotated by the current. The nacelle is used to accommodate the PMSGs, an encoder, and other components [31]. The diameter of the blade is 1 m and the distance between two nacelles is 1.5 m which are decided by the results of fluid dynamic simulation. According to the simulation, the distance can make the FKT more stable during the operation. The goal of the FKT is to generate 800 W of power output at a flow rate of 1.5 m/s.

The effect of surface waves in the open ocean is considered for the structure of the floating turbine. When the generator operates, the floating turbine will dive into the sea due to the towing rope and pressures as shown in Figure 22 so that the waves have no effect on FKT during the operation; when the floating turbine does not operate, it will float on the surface due to the buoyancy of the foil float structure as shown in Figure 23, so that it is easy for maintenance.

4.2 | Experiment results

Figures 24 and 25 show the power generated by two PMSGs during a towing tank experiment. The PMSGs were towed at different rotation speeds at a load of 182, 262, 364, and 728 Ohms. The different rotation speeds corresponded to a carriage speed between 0.7 and 1.5 m/s, as shown in Figures 26 and 27, which is approximately the flow rate of the Kuroshio current off the eastern coast of Taiwan. In the FKT system, the turbine begins operating once the flow rate rises above 0.7 m/s. The DC power output of the two PMSGs will be near to 400 W at a carriage speed of 1.5 m/s. For PMSG-2, the output power at a load of 182, 262 and 364 Ohms can exceed 400 W. The output power can even increase to up to 466, 456, or 440 W when the rotation speed reaches 150 rpm corresponding to a carriage speed of 1.5 m/s, as shown Figures 26 and 27. For PMSG-1, the output power at a load of 182, 262, and 364 Ohms is about 380 W. The connecting parts installed in each PMSG may cause different power losses.

According to Figures 24–27, the relationships between rotation speed, carriage speed, flow speed and power output are shown.

Figures 26 and 27 show the rotation speed as a function of the flow rate for four different loads. The rotation speed was recorded by the encoder in the nacelle under the water as the

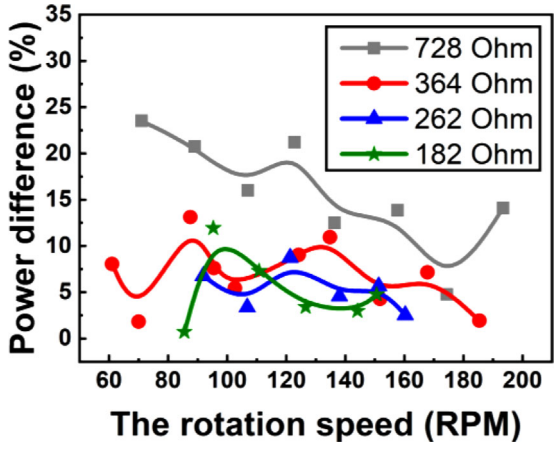

FIGURE 28 Difference in power between the testing platform and the towing experiments for PMSG-1

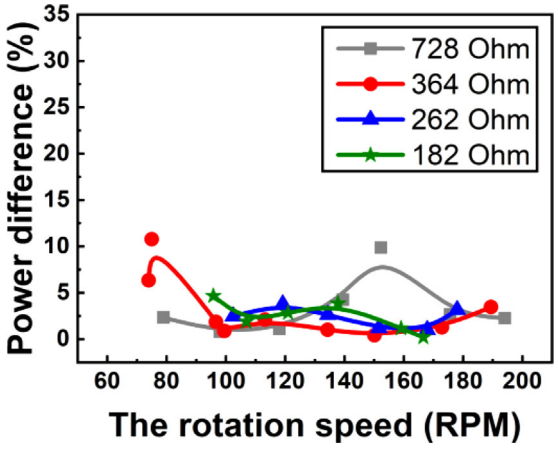

FIGURE 29 Difference in power between the testing platform and the towing experiments for PMSG-2

current flows through the FKT. These curves clearly show the relationship between the flow rate and the rotation speed. In the towing tank, the FKT system starts working at flow rates between 0.7 and 1.5 m/s at a load of 728 Ohms, and then from a flow rate of between 0.75 and 1.5 m/s at a load of 364 Ohms, then from flow rates between 1 and 1.5 m/s at a load of 262 Ohms, and finally from flow rates between 1.05 and 1.5 m/s at a load of 182 Ohms.

The slopes for the eight curves illustrated in Figures 26 and 27 are almost the same, about 173(rpm × s/m), and are linearly dependent on the increasing flow rate. However, at the same flow rate, the rotation speed at different loads is higher for PMSG-2 than for PMSG-1 due to the difference in torque for the PMSGs and the connecting parts in the nacelle.

$$Power_{difference}(\%) = \frac{P_{testing} - P_{towing}}{P_{testing}} \quad (4)$$

Figures 28 and 29 show the difference in power between the testing platform and the towing experiment for the same rotation speed by using Equation (4). As can be seen from the curves for PMSG-2, the difference is more stable, approximately below 5%. However, PMSG-1 has a greater difference, between 5% and 10%, although the difference is between 15% and 25% when the load is 728 Ohms. The reasons for the difference in power between the two PMSGs should be the same as mentioned before. The difference in power for the rated rotation speed at a load of 182 Ohms has the lowest value, that is, 5%.

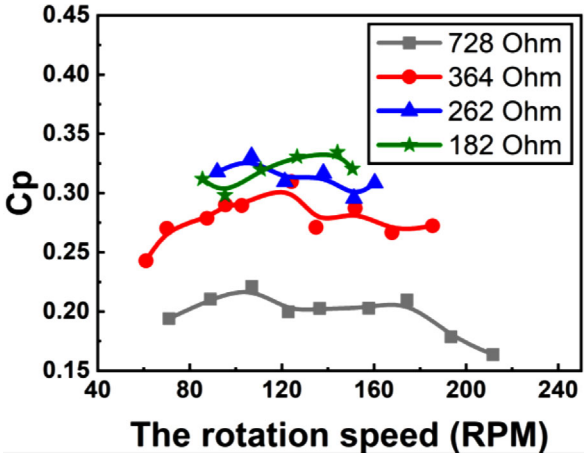

FIGURE 30 Energy conversion efficiency for PMSG-1 in the FKT system from the towing experiments with four loads

At the same rotation speed, the produced voltage is about the same. Therefore, when the load resistance decreases, the current will increase, leading to higher power output. However, the current value is limited by the power line and rated power (400 W). The lowest resistance used in this research is close to the limit to obtain maximum power. In addition, comparing the resistance range between 182 and 728 Ohm for 800 W in this research and the resistance of 160 Ohm for 959 W in the reference [30], the resistance used in this research should be suitable. The optimal resistance of the load will be studied later.

Figures 30 and 31 show the power coefficient (C_p) for the PMSGs installed in the FKT from the towing experiments, which are calculated from the input energy and the output energy. The input energy is the current energy flowing through the FKT system, and the output energy is the electrical energy generated by the PMSGs seen Equation (5). The calculation of current energy is the same as wind energy, so the equation of wind energy is listed below. The experiments were performed at different rotation speeds that are corresponded to the carriage speeds at loads of 728, 364, 262, and 182 Ohms. Observing the figures, the power coefficients for PMSG-1 and PMSG-2 can reach 0.32 and 0.4, respectively. The power coefficient for PMSG-2 is about 0.4 between 90 and 170 rpm at a load of 182 Ohms, and the power coefficient for PMSG-1 is 0.32 near the rated rotation speed at a load of 182 Ohms. This means that the power coefficient for the FKT system can be high and stable if the design and the assembly are well arranged.

$$P = \frac{1}{2}\rho A V^3 C_p \quad (5)$$

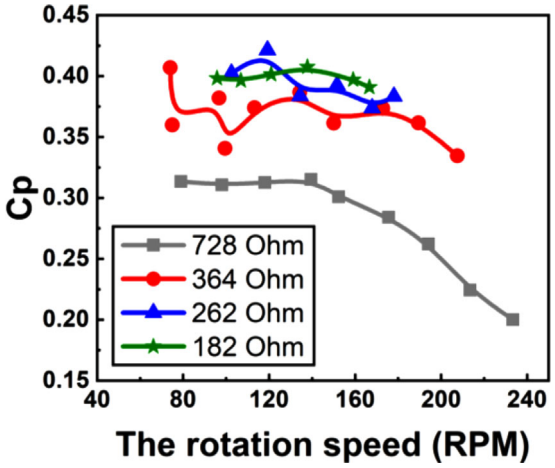

FIGURE 31 Energy conversion efficiency for PMSG-2 in the FKT system from the towing experiments with four loads

where P is power output; ρ is sea water density; A is the circle area of a blade; V is the current flow rate and C_p is power coefficient.

5 | CONCLUSION

In this study, a new type of a marine current turbine, the Floating Kuroshio Turbine, was designed to harvest the kinetic energy from Kuroshio currents. The depth for the FKT system can be adjusted, dependent on the current flow rate and the weather conditions, leading to a longer lifetime and lower cost of maintenance. In order to develop the generators for the FKT system, ANSYS Maxwell software was used to design and simulate a 400 W low-speed direct-drive PMSG. The simulation results show that the PMSG generates 398 W in a DC environment (270 V and 1.48 A) at a rotation speed of 150 rpm and a load of 182 Ohms. The maximum magnetic flux density is about 2.1 Tesla. In addition, the 400 W low-speed direct-drive PMSGs was tested by using the testing platform at rotation speeds between 30 and 150 rpm. Consequently, the generated AC power output for the two PMSGs was 417 and 411 W. After introducing a rectifier circuit with an internal resistance of 15 Ohms, the DC output for the two PMSGs became 398 and 388 W. Furthermore, we compared the power loss in each stage, including the internal loss and the AC-DC conversion loss. The power loss between the input and the AC output is 15.6% and 7.8%, at a load of 182 Ohms at 150 rpm for PMSG-1 and PMSG-2, respectively. The power loss between the AC output and the DC output is 6% and 4.3% at a load of 182 Ohms at 150 rpm for PMSG-1 and PMSG-2, respectively. The total power loss between the input and the DC output amounts to 19.3% and 13.3% at 150 rpm at a load of 182 Ohms for PMSG-1 and PMSG-2, respectively. The energy conversion efficiency of the two PMSGs is about 0.80 and 0.85 at the rated rotation speed. Moreover, the error between the simulated and the measured DC power output by the PMSG is 7.7% at a load of 728 Ohms, reduced to 0.3% at a load of 182 Ohms at 150 rpm. Finally, the experiments for the FKT were conducted in a towing tank at carriage speeds from 0.7 to 1.5 m/s. The measured power output by the two PMSGs was 466 and 382 W, and the total DC output power was 848 W at a speed of 1.5 m/s. The difference in power between the testing platform and the towing experiment at the same rotation speed was about 5–10% at the rated rotation speed. The average power coefficient for the two PMSGs was about 0.32 and 0.4, respectively, at a load of 182 Ohms. This means that the efficiency of the FKT is high and stable. The novel FKT is highly suitable for harvesting marine energy.

AUTHOR CONTRIBUTIONS

P.-Y.C.: Writing—original draft. K.-Y.L.: Supervision; Validation; Writing—original draft; Writing—review and editing. P.-C.H.: Validation; Writing—original draft; Writing—review and editing. J.-H.L.: Methodology. F.-C.C.: Methodology. J.-F.T.: Methodology. S.-T.H.: Writing—original draft.

ACKNOWLEDGEMENTS

This work was supported in part by the Ministry of Education's Higher Education Sprout Project under the Featured Area Research Center Program under the contract NO. 111L9006 and the National Science and Technology Council, Taiwan, under the contract NO. NSTC 111-2634-F-002-016, MOST 111-2218-E-002-024, 110-2221-E-002-173-MY3, 110-2218-E-194-007, 110-2823-8-002-001, 108-3017-F-002-002, and 106-3113-E-002-002-cc2.

FUNDING INFORMATION

Ministry of Education's Higher Education Sprout Project under the Featured Area Research Center Program under the contract NO. 111L9006 and the National Science and Technology Council, Taiwan, under the contract NO. NSTC 111-2634-F-002-016, MOST 111-2218-E-002-024, 110-2221-E-002-173-MY3, 110-2218-E-194-007, 110-2823-8-002-001, 108-3017-F-002-002, and 106-3113-E-002-002-cc2.

CONFLICT OF INTEREST

The authors declare that they have no known competing financial interests or personal relationships that could have appeared to influence the work reported in this paper.

DATA AVAILABILITY STATEMENT

The data that support the findings of this study are available from the corresponding author upon reasonable request. cd_value_code=text

ORCID

Kung-Yen Lee https://orcid.org/0000-0003-2590-0702

REFERENCES

1. Isaka, M.: Water desalination using renewable energy. International Renewable Energy Agency (2012)
2. Borthwick, A.G.L.: Marine renewable energy seascape. Engineering 2(1), 69–78 (2016)

3. Zhou, Z., Benbouzid, M.E.H., Charpentier, J.F., Scuiller, F., Tang, T.-H.: Developments in large marine current turbine technologies – A review. Renewable Sustainable Energy Rev. 71, 852–858 (2017)
4. Zhou, Z., Scuiller, F., Charpentier, J.F., Benbouzid, M., Tang, T.: An up-to-date review of large marine tidal current turbine technologies. In: 2014 International Power Electronics and Application Conference and Exposition. Shanghai, China (2014)
5. Liang, W.-D., Tang, T.Y., Yang, Y.J., Ko, M.T., Chuang, W.-S.: Upper-ocean currents around Taiwan. Deep Sea Res. Part II 50, 1085–1105 (2003)
6. Kaneko, A., Mizuno, S., Koterayama, W., Lee Gordon, R.: Cross-stream velocity structures and their downstream variation of the Kuroshio around Japan. Deep Sea Res. Part A 39(9), 1583–1594 (1992)
7. Imamura, J.T., Takagi, K., Waseda, T., Kiyomatsu, K.: Kuchinoshima island ocean current measurements for Kuroshio current energy. In: OCEANS 2016 MTS/IEEE Monterey, Monterey (2016)
8. Yang, X., Haas, K.A., Fritz, H.M.: Evaluating the potential for energy extraction from turbines in the Gulf stream system. Renewable Energy 72, 12–21 (2014)
9. Yang, X., Haas, K.A., Fritz, H.M., French, S.P., Shi, X., Neary, V.S., Gunawan, B.: National geodatabase of ocean current power resource in USA. Renewable Sustainable Energy Rev. 44, 496–507 (2015)
10. Driscoll, F., Skemp, S., Alsenas, G., Coley, C., Leland, A.: Florida's Center for Ocean Energy Technology. OCEANS 2008. pp. 1–8 (2008)
11. Rourke, F.O., Boyle, F., Reynolds, A.: Marine current energy devices: Current status and possible future applications in Ireland. Renewable Sustainable Energy Rev. 14(3), 1026–1036 (2010)
12. Shirasawa, K., Tokunaga, K., Iwashita, H., Shintake, T.: Experimental verification of a floating ocean-current turbine with a single rotor for use in Kuroshio currents. Renewable Energy 91, 189–195 (2016)
13. Corporation, I.: Development of floating type ocean current turbine system in power generation using the Kuroshio current. IHI Eng. Rev. 46(2), 2–5 (2014)
14. New Energy and Industrial Technology Development Organization. Prototype for "subsea floating type ocean current power generation" completed that utilizes a new type of renewable energy technology (2017) http://www.nedo.go.jp/english/news/AA5en_100269.html. Accessed on: 2017
15. Ueno, T., Nagaya, S., Shimizu, M., Saito, H., Murata, S., Handa, N.: Development and demonstration test for floating type ocean current turbine system conducted in Kuroshio current. In: 2018 OCEANS - MTS/IEEE Kobe Techno-Oceans (OTO) (2018)
16. Imamura, J.T., Takagi, K., Waseda, T.: Turbulence measurements near Kuchinoshima Island for Kuroshio current energy. In: OCEANS 2017 - Anchorage (2017)
17. Takagi, K., Suyama, Y., Kagaya, K.: An attempt to control the motion of floating current turbine by the pitch control. In: OCEANS'11 MTS/IEEE KONA (2011)
18. Takagi, K., Waseda, T., Nagaya, S., Niizeki, Y., Oda, Y.: Development of a floating current turbine. OCEANS 2012. pp. 1–5 (2012)
19. Shibata, M., Takeda, K., Takagi, K.: Mooring and power cable system for current-turbine. In: 2013 OCEANS - San Diego (2013)
20. Gonoji, T., Takagi, K., Takeda, K.: Motion of twin type ocean current turbine at the time of startup and accident. In: 2013 OCEANS - San Diego (2013)
21. Sakata, K., Gonoji, T., Takagi, K.: A motion of twin type ocean current turbines in realistic situations. In: 2012 Oceans - Yeosu (2012)
22. Chen, Y.Y., Hsu, H.C., Bai, C.Y., Yang, Y., Lee, C.W., Cheng, H.K., Shyue, S.W., Li, M.S., Hsu, C.J.: Evaluation of Test Platform in the Open Sea and Mounting Test of Kw Kuroshio Power-Generating Pilot Facilities. Taiwan Wind Energy Association (2016)
23. Wei, L., Nakamura, T., Imai, K.: Development and optimization of low-speed and high-efficiency permanent magnet generator for micro hydro-electrical generation system. Renewable Energy 147, 1653–1662 (2020)
24. Tanigaki, S., Ishida, H., Sugiyama, S., Asano, S., Sakata, N.: Development of ocean current marine turbine. IOP Conf. Ser.: Earth Environ. Sci. 240, 052012 (2019)
25. Han, X., Su, W., Zhao, H., Zheng, Y., Hu, Q., Wang, C.: Research of the hydrostatic transmission for deep-sea current energy converter. Energy Convers. Manage. 207, 112544 (2020)
26. Jiang, B., Li, X., Chen, S., Xiong, Q., Chen, B.-F., Parker, R.G., Zuo, L.: Performance analysis and tank test validation of a hybrid ocean wave-current energy converter with a single power takeoff. Energy Convers. Manage. 224, 113268 (2020)
27. Weiss, C.V.C., Guanche, R., Ondiviela, B., Castellanos, O.F., Juanes, J.: Marine renewable energy potential: A global perspective for offshore wind and wave exploitation. Energy Convers. Manage. 177, 43–54 (2018)
28. Dubois, M., Polinder, H., Ferreira, J.A.: Comparison of generator topologies for direct-drive wind turbines. Nordic Countries Power and Industrial Electronics Conference (NORPIE), (2000)
29. Grauers, A.: Design of direct driven permanent magnet generators for wind turbines. Chalmers University of Technology. Department of Electric Power Engineering. (1996)
30. Juan, Y.W.: Design of the Permanent Magnet Synchronous Generator and Simulation of the Power System for Kuroshio Current. M.S., National Taiwan University (2017)
31. Liao, Y.H.: Hydrodynamic Performance of a Towed Floating Kuroshio Current Turbine. M.S., National Taiwan University (2018)

How to cite this article: Chen, P.-Y., Lee, K.-Y., Huang, P.-C., Li, J.-H., Chiu, F.-C., Tsai, J.-F., Hsu, S.-T.: The performance analysis of the low-speed direct-drive generators for harvesting current energy. IET Renew. Power Gener. 1–12 (2022). https://doi.org/10.1049/rpg2.12598